Journal of Applied Fluid Mechanics, Vol. 18, No. 12, pp. 3036-3052, 2025.
Available online at www.jafmonline.net, ISSN 1735-3572, EISSN 1735-3645.
https://doi.org/10.47176/jafm.18.12.3577

Study on the Cavitation Performances and Unsteady Characteristics of a Centrifugal Fire Pump

J. Hao[1], C. Yu[1], Y. Fu[2†], P. Zhang[1], D. Hou[3], Y. Shen[4] and J. Yuan[1]

[1] *National Research Center of Pump, Jiangsu University, Zhenjiang 212013, Jiangsu, China*
[2] *School of Energy and Power Engineering, Jiangsu University, Zhenjiang 212013, Jiangsu, China*
[3] *Shanghai Kaiquan Pump (Group) Co. Ltd., Jiading 4255/4287, Shanghai, China*
[4] *Zhenjiang Fire and Rescue Division, Zhenjiang 212000, Jiangsu, China*

†*Corresponding Author Email: yanxiafu@ujs.edu.cn*

ABSTRACT

Centrifugal fire pumps are critical for firefighting systems but suffer from cavitation and instability under off-design conditions. However, systematic analyses of their flow-rate-dependent dynamics remain limited. This study systematically investigates the hydraulic performance, cavitation characteristics, and dynamic pressure pulsations of a centrifugal fire pump under various flow conditions (50%–150% of the design flow rate) through combined numerical simulations and experiments. Steady simulations were conducted using the standard κ-ε turbulence model, while unsteady simulations were performed with a 2° angular time step to capture the transient interactions between the impeller and the volute as well as the resulting dynamic pressure pulsations. Key results revealed that: At low flow (60% Q_d), Radial force amplitudes increased by 40%, accompanied by 9.86 Hz low-frequency pulsations attributed to backflow-induced instabilities; At high flow (150% Q_d), The critical cavitation number σ_3% surged to 0.961, indicating a 2.6-fold cavitation risk compared to the design condition (σ_3% = 0.376); The findings provide actionable strategies for optimizing pump design and operational stability in firefighting systems.

Article History

Received April 11, 2025
Revised June 5, 2025
Accepted July 9, 2025
Available online October 6, 2025

Keywords:

Centrifugal fire pump
Hydraulic performance
Cavitation performance
Hydraulic forces
Unsteady characteristics
Pressure pulsation
Numerical simulation

1. INTRODUCTION

The estimated annual cost each year due to unintentional fire losses is approximately 1% of global Gross Domestic Product (GDP). Fire safety merits serious attention worldwide due to the increasing data on global fire deaths, injuries and damage and must be part of any national disaster risk reduction management (International Association of Fire and Rescue Services (CTIF), 2014). With the growing importance of fire safety, the demand on efficient firefighting equipment is in rise. Among the essential components of firefighting systems, fire pumps plays a vital role in enhancing the performances of firefighting facilities in the emergency response system. These pumps are extensively used for a wide range of liquid transfer operations within firefighting applications, contributing significantly to the reliability and performance of fire suppression systems. The effectiveness of fire pumps is largely determined by their design. Among the various types of pumps, centrifugal fire pumps are the most commonly used in modern firefighting systems. Due to their relatively flat characteristic performance curves, centrifugal fire pumps can provide a relatively stable pressure and flow rate across a wide range of working conditions, and are routinely designated as critical equipment for fire water transfer in industrial facility protection worldwide (Palgrave & Ron, 2003). Moreover, centrifugal fire pumps have the advantages of a compact structure, easy starting, high efficiency and low maintenance requirements, and have been also widely used for both onshore and offshore or even underground facilities (Nolan, 2011).

However, centrifugal pumps also have certain drawbacks, such as, one of the undesired flow phenomena, cavitation can occur in a centrifugal fire pump, the internal flow inside blade passages with the most complex structure will become extremely unstable especially at lower flow rates, together with increasing vibration and noise (Brennen, 2012). The poor inner flow or deteriorated performances in a cavitating centrifugal fire pump can cause an inefficient water supply and transfer or even a failure to a firefighting system, and is therefore a potential threat to property and human life during emergency fire-rescue situations. Therefore, more investigative efforts are required to understand performances and dynamic

NOMENCLATURE

Z_1	blade number of the impeller	f_n	shaft rotating frequency
Ψ	total pressure rise coefficient	f_b	blade passing frequency
ρ	fluid density	σ	cavitation number
p_1	total pressure obtained at pump inlet	p_{in}	inlet pressure
p_2	total pressure obtained at pump outlet	u_1:	mean velocity at the impeller inlet
η	hydraulic efficiency	t	time
Q	volumetric flow	k	turbulence energy
ω	angular velocity	ε	dissipation rate
p_v	saturation vapor pressure	n_s	impeller specific speed
C_p	static pressure coefficient	$\sigma_{3\%}$	cavitation number related to a head-drop amount equal to 3%
$\overline{p}$:	average static pressure		

characteristics in a non-cavitating and cavitating centrifugal fire pumps. So far, a number of researchers over the years have been dedicated to study the improvement of pumping or suction performance of pumps based on different design optimization methods. For instance, (Elyamin et al., 2019) numerically investigated the impact of blade number on pumping performances, and they revealed that the optimal performance could be achieved using 7 blades with improved secondary flow and less flow losses. Yousefi et al. (2019) studied the impact of blade angles and blade edge shapes on secondary flows and energy efficiency. Oro et al. (2023) investigated the impact of the radial clearance on pumping performances and internal flow in centrifugal pumps at different flow rates. Bozorgasareh et al. (2021) found the auxiliary impeller can increase the pump head and efficiency when designing a semi-open impeller. Skrzypacz & Bieganowski (2018) found that hydraulic losses in a centrifugal pump could be reduced by modifying the blade passages with micro-grooves. Recent advancements in computational and experimental methodologies have significantly deepened the understanding of unsteady cavitation dynamics and flow instabilities in centrifugal pumps. Osman et al. (2022) used ANSYS CFX with URANS to numerically study vertical fire pumps, investigating the effects of turbulence models on unsteady flow characteristics. The study providing a theoretical reference for complex three-dimensional unsteady flow analysis. Jia et al. (2024) established quantitative correlations between cavitation degree and pressure pulsation amplitudes, showing that radial force fluctuations intensify with cavitation development, particularly in high-frequency bands. Lu et al. (2023) investigated quasi-steady cavitation-induced pressure pulsations using wavelet analysis and dynamic mode decomposition (DMD), identifying dominant blade passing frequency (BPF) effects and validating numerical results with experimental data. Song et al. (2024) proposed a cavitation identification method combining signal demodulation and EfficientNet, achieving 89.44% recognition accuracy and outperforming traditional FFT-based approaches by 20.69%. For design optimization, Liu et al. (2024) developed an OpenFOAM-based multiphase flow model for aviation centrifugal pumps, reducing cavitation number prediction errors to 3.7% compared to experimental tests. Sonawat et al. (2022) found that the occurrence of cavitation phenomenon has a significant impact on pumping performances and inner flow fields inside double-suction centrifugal pumps with different specific speeds based on the relevant experimental and numerical data obtained by using the open-source CFD software OpenFoam. Zhu et al. (2023) comprehensively reviewed the identification and suppression methods for monitoring the cavitation state of centrifugal pumps. They discussed various cavitation monitoring methods and signal characterization techniques, providing valuable insights for predictive maintenance. Experimental innovations further bridge theory and practice. Dai et al. (2022) experimentally characterized noise variations across cavitation stages in marine centrifugal pumps, revealing that broadband noise energy concentrates in high frequencies (>1000 Hz) during severe cavitation, with a 10% reduction in 2BPF sound pressure levels under fan sound sources. Huan et al. (2021) analyzed cavitation evolution in high-speed pumps with inducers, linking vapor distribution to static pressure changes and providing insights for inducer design. Lu et al. (2022) combined Q-criterion analysis and experiments to detect flow instabilities in centrifugal pumps, identifying rotating stall and leakage vortices as key contributors to pressure fluctuations. Long et al. (2021) utilized high-speed photography and numerical simulations to explore cavitation-vortex interactions in water-jet pumps, emphasizing velocity isosurface dynamics. However, there has been no large-scale investigation demonstrating that the operation reliability in cavitating centrifugal fire pumps are clearly related to its dynamic characteristics at different flow rates. As mentioned, cavitation can directly affect the inner flow, thus influencing the pumping and suction performances of a centrifugal fire pump. Therefore, it is necessary to investigate the dynamic characteristics and its relationship with the operating reliability of a centrifugal fire pump running under different working conditions to reduce their power consumption and enhance overall performances.

The current computational fluid dynamics (CFD) can typically provide the level of accuracy required to predict various cavitating flows in engineering fields. Recently, it has become widely used in research on fluid machinery as a design tool. Meanwhile, the development of computer technology allows for the use of advanced turbulent models to simulate geometrically complex centrifugal pumps. Although, due to the complexities involved in the cavitation phenomenon and the limited development of current turbulence models as reported in previous

literature works, only limited numerical research on cavitation characteristics of centrifugal fire pumps working specially under off-design flow conditions, have been available online up to now (Fu, et al. 2016, 2018; Ramirez, et al. 2020).

The objective of the present research was to assess the possibility of recreating the flow fields in a centrifugal fire pump across a range of flow rates via steady and unsteady numerical simulations. Steady simulations, based on Reynolds-Averaged Navier-Stokes equations with a Frozen Rotor interface, were conducted to obtain time-averaged flow fields and hydraulic performances. Concurrently, unsteady simulations employing a Transient Rotor-Stator interface with a 2° angular time step were performed to resolve transient impeller-volute interactions and capture resultant dynamic pressure pulsations and hydraulic forces. The non-cavitation and cavitation performances, hydraulic forces and pressure fluctuations within the model centrifugal fire pump operating under various flow conditions were predicted based on *k-ε* and *SST k-ω* turbulence models using ANSYS CFX (ANSYS Inc, 2012) installed in High-Performance Computing Clusters Systems of Jiangsu University (Fu, et al. 2018). Pressure pulsations inside the fire pump impeller and volute were further analyzed by means of studying the distributions of time and frequency domains. Additionally, a series of hydraulic performance tests were conducted on the tested centrifugal fire pump based upon the test rig set up in the laboratory of KQ PUMPS, Shanghai, China, which is a versatile and easy-to-install appliance and also easily adjusted to accomplish research on essentially any fluid flow problems involved in multi-scale hydraulic models of pumps and turbines in a large number of alternative arrangements. Particularly, the technical specifications of the hydraulic performance test rigs at KQ PUMPS are considered to be at an advanced level within China. Furthermore, the hydraulic performance experiment was performed for the investigated centrifugal fire pump, and the relevant test results were also compared with the predicted ones for validation.

2. MODELING AND NUMERICAL METHOD

2.1 Geometrical Data

The model centrifugal fire pump used in this study is commonly applied in firefighting applications and was employed in both experiments and numerical simulations maintaining same dimensions and geometric configurations. As illustrated in Fig. 1, the computational model of the complete centrifugal fire pump was developed using UG software, it includes a five-bladed impeller, a volute and the inlet and outlet pipes with their extended portions (4 diameters upstream and 5 diameters downstream to account for inlet pre-rotation or secondary flow in the pipelines under partial working conditions. These extensions ensure accuracy in the simulation by mitigating boundary influence in cases where the pipe lengths are insufficient. The relevant design and geometric parameters of the investigated centrifugal fire pump are presented in Table 1.

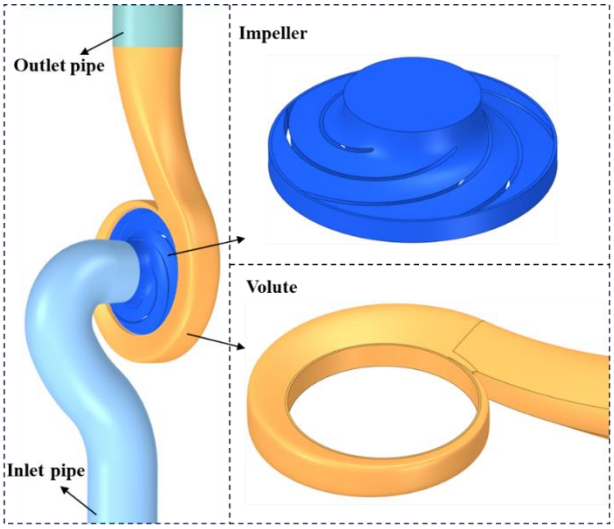

Fig. 1 Computational domain of the model pump

Table 1 Design and geometrical parameters of the impeller

Parameters	Symbols	Value	Units
Design flow rate	Q_d	144	m^3h^{-1}
Design head	H_d	52	m
Rotational speed	n	2960	rpm
Specific speed	n_s	115	[--]
Blade number of the impeller	Z_1	5	[--]
Impeller inlet diameter	D_1	0.07	m
Impeller outlet diameter	D_2	0.225	m
Diameter of inlet pipe	D_s	0.125	m
Diameter of outlet pipe	D_d	0.125	m
Inlet pipe length	L_s	0.5	m
Outlet pipe length	L_d	0.625	m

2.2 Mesh Independence Analysis

Compared with unstructured tetrahedral cells, structured hexahedron cells are more acceptable to researchers with advantages of wider adaptability to the complex flow channels and generating better-quality mesh with smaller truncation errors. Consequently, the numerical mesh for the investigated fire pump, including its twisted blades, was generated using structured hexahedral grids with ANSYS ICEM CFD software. Although a refiner mesh can improve the convergence and increase numerical accuracy, it also demands greater computational resources. Therefore, it was necessary to optimize the mesh size consistent with the results of a mesh sensitivity check to choose the most appropriate mesh to predict the inner flow in the model investigated fire pump in the present study. Furthermore, the boundary layer close to the wall was created to better capture the complex flow phenomena near to the blade surfaces. This was achieved by setting the first grid height to 0.02 mm with an expansion ratio of 1.2. The mesh quality across all cases exceeded 0.5, indicating satisfactory mesh integrity. In addition, the minimum values of y+ in the calculation domain were approximately 10, which is appropriate for

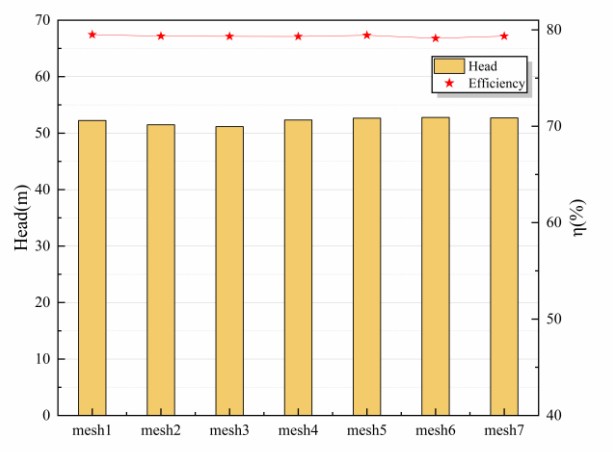

Fig. 2 Comparison of performance data of the model fire pump among different mesh schemes

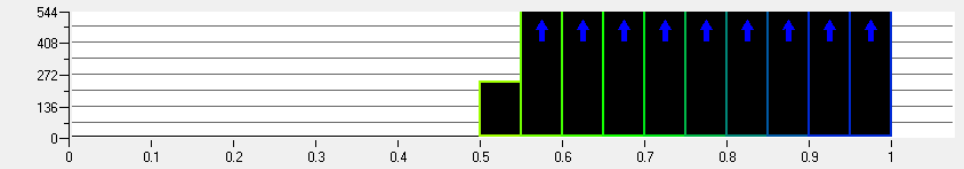

(a) Mesh quality distribution

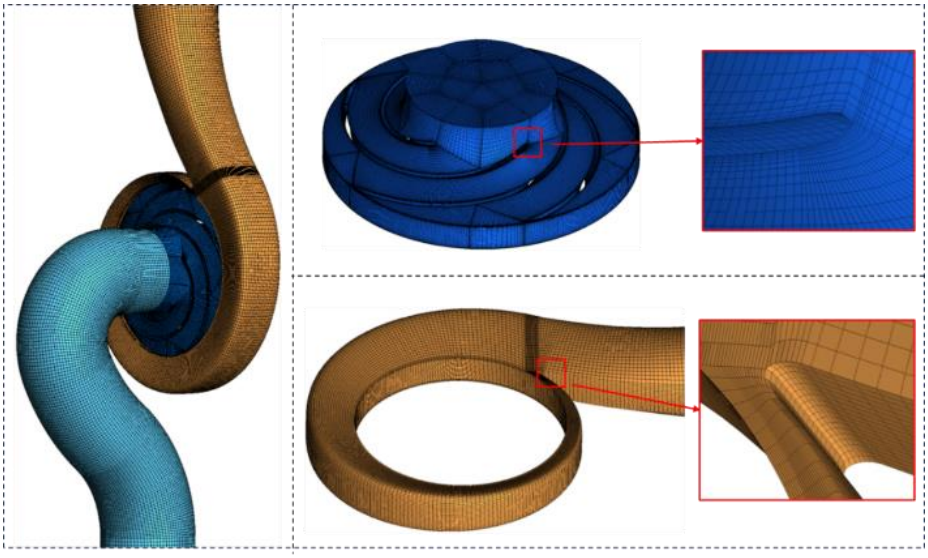

(b) Grids of the main computational domains

Fig. 3 Mesh information for the model centrifugal fire pump

Table 2 Details of mesh information for the centrifugal fire pump

Mesh Cases	Mesh Elements	
mesh 1	403,364	
mesh 2	463,667	
mesh 3	1,001,826	
mesh 4	2,046,208	
mesh 5	2,987,569	
mesh 6	4,177,788	
mesh 7	4,887,075	

the application of the selected standard κ-ε and SST k-ω turbulence models used in this numerical work.

In particular, as displayed in Table 2, seven mesh cases with different mesh numbers were chosen for the whole computational domain of the model fire pump. This was done to investigate the effect of mesh size on the prediction of hydraulic performance at the design operating point, based on steady-state numerical simulations. As the mesh element count was increased from 0.4 million to 4.8 million, further comparative analysis was conducted on the numerical results of pump head and hydraulic efficiency. Figure 2 shows that the seven mesh schemes all exhibit small deviations in head and efficiency from the model pump's design parameters. To balance computational accuracy and resource efficiency, Mesh Case 2 was selected. The overall mesh of the centrifugal fire pump model is presented in Fig. 3.

2.3 Turbulence Models and Boundary Conditions

The turbulent flow inside the centrifugal fire pump running under different flow conditions was numerically calculated in ANSYS CFX by means of Reynolds-averaged Navier-Stokes equations coupled with standard κ-ε, RNG k-ε and SST k-ω turbulence models which are widely used in practical engineering for flow analyses. With the fluid being assumed to be incompressible and homogeneous, the governing equations are as follows,

$$\frac{\partial \rho}{\partial t} + \nabla \cdot \left(\rho u_j\right) = 0 \tag{1}$$

$$\frac{\partial(\rho u_i)}{\partial t} + \frac{\partial(\rho u_i u_j)}{\partial x_j} = -\frac{\partial p}{\partial x_i} + \frac{\partial}{\partial x_j}\left[(\mu + \mu_t)\left(\frac{\partial u_i}{\partial x_j} + \frac{\partial u_j}{\partial x_i} - \frac{2}{3}\frac{\partial u_k}{\partial x_k}\delta_{ij}\right)\right] \tag{2}$$

$$\rho = \sum_{c=1}^{N_p} \alpha_c \rho_c \tag{3}$$

$$\mu = \sum_{c=1}^{N_p} \alpha_c \mu_c \tag{4}$$

where u is the velocity, p is the pressure, ρ is the mixture density, μ is the viscosity, α_c is the phasic volume fraction and N_p is the number of phases.

The impact of these three different turbulence models on prediction of the fire pump's performance was evaluated by comparing the simulation results with experimental data to assess their computational accuracy. The turbulence model in this paper adopts the standard k–ε model. the expression of this model is:

$$\rho\frac{\partial k}{\partial t} + \rho u_j \frac{\partial k}{\partial x_j} = \tau_{ij}\frac{\partial u_i}{\partial x_j} - \rho\varepsilon + \frac{\partial}{\partial x_j}\left(\left(\mu + \frac{\mu_t}{\sigma_k}\right)\frac{\partial k}{\partial x_j}\right) \tag{5}$$

$$\rho\frac{\partial \varepsilon}{\partial t} + \rho u_j \frac{\partial \varepsilon}{\partial x_j} = C_{e1}\frac{\varepsilon}{k}\tau_{ij}\frac{\partial u_i}{\partial x_j} - C_{e2}\rho\frac{\varepsilon^2}{k} + \frac{\partial}{\partial x_j}\left(\left(\mu + \frac{\mu_t}{\sigma_\varepsilon}\right)\frac{\partial \varepsilon}{\partial x_j}\right) \tag{6}$$

Where the model constants can be assigned as: $C_{\varepsilon 1} = 1.44$, $C_{\varepsilon 2} = 1.92$, $C_\mu = 0.09$, $\sigma_k = 1.0$, $\sigma_\varepsilon = 1.3$.

Moreover, all boundaries are assumed to have no-slip conditions. Scalable wall functions were applied with the high-resolution scheme chosen to discretize convective and diffusion terms. The frozen rotor mode was utilized for pitch changes of the interfaces between the inlet pipe and the impeller, as well as between the impeller and the volute, throughout all steady-state simulations. Water at 25°C was used to the working fluid. The inlet total pressure and outlet mass flow rate were imposed as the boundary conditions for the model pump among all operating flow rates, respectively. The convergence criterion for the residual value was set to a magnitude below 10^{-7}.

In addition, the unsteady flow inside the centrifugal fire pump operating at lower, design and higher flow rates were numerically simulated to evaluate the dynamic characteristics. The pitch change between the rotor and stator interface was defined as transient rotor-stator. Moreover, all unsteady simulations were initialized based on the converged steady results of the corresponding calculations at the same flow rates.

Considering that the accuracy of the transient results can be affected by the temporal resolution, such as the time steps selected during the unsteady numerical simulations, one full rotation of the model fire pump operating at the design flow point was therefore discretized by 1200, 360, 180, 120 and 72 time steps. These correspond to the angular changes of 0.3°, 1.0°, 2.0°, 3.0° and 5.0° for per time step, respectively. The associated time steps were 1.689E-05s, 5.631E-05s, 1.126E-04s, 1.689E-04s and 2.815E-03s, respectively. For each flow rate investigated, unsteady flow was simulated over eight full rotor revolutions, with data from the final full rotation extracted for subsequent FFT analysis.

2.4 Time Step Independence Check

As for the time step independence check, the calculated head coefficient and hydraulic efficiency of the model fire pump operating at the design flow point has been analyzed with respect to the selected five different time steps as mentioned above, and the corresponding results corresponding to each time step are displayed in Fig. 4.

As the time step increases from the corresponding angular change of 0.3 degree to 5 degrees, the total pressure rise coefficient and hydraulic efficiency at the investigated flow rate, remain almost in accordance with the experimental results with a small and acceptable deviation which is less than 2%. Especially, the minimum deviation of 0.06% was obtained for the particular time step related to an angular change of 2 degrees, where the minimum deviation of the hydraulic efficiency with the value of 0.75% was achieved as well. Clearly, the predicted total pressure rise coefficient and hydraulic efficiency agree well with the experimental data at the design condition using the time step relate to an angular change of 2 degrees applied in unsteady calculations.

To ensure the calculated accuracy, reduce the consuming time, and save computational resources at the same time, a medium time step size corresponding to the angular change of 2 degrees was selected for further unsteady numerical simulations.

2.5 Numerical Methods for Cavitation Flow

With respect to the cavitation flow in the model fire pump, the Navier-Stokes equations concerning about the appearance of liquid and vapor phases was numerically solved using ANSYS CFX. The Rayleigh-Plesset cavitation model was applied to estimate interphase mass transfer effects, and essentially assimilates the cavitating liquid to a homogeneous vapor and liquid mixture. The Rayleigh-Plesset equation is expressed as follows，

$$R_b\frac{d^2R_b}{dt^2} + \frac{3}{2}\left(\frac{dR_b}{dt}\right)^2 + \frac{4\mu}{\rho_l R_b}\frac{dR_b}{dt} + \frac{2S}{\rho_l R_b} + \frac{p_\infty(t) - P_b}{\rho_l} = 0 \tag{7}$$

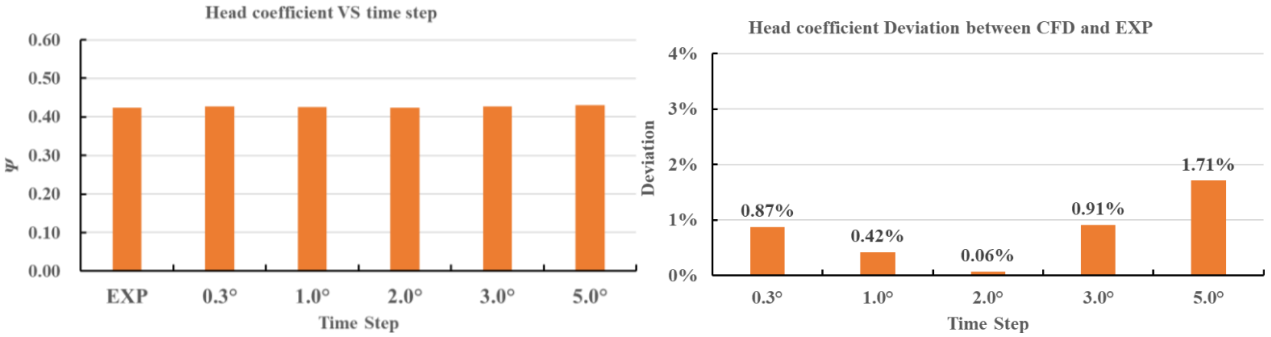

(a) Head coefficient at the design point.

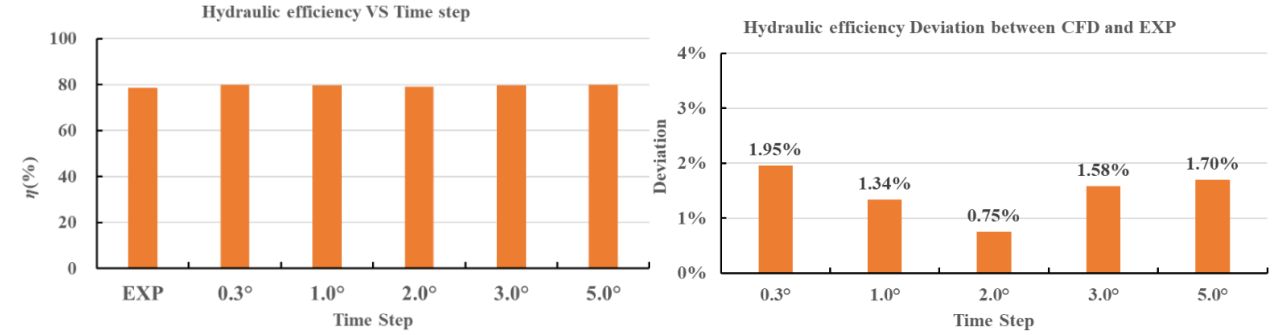

(b) Hydraulic efficiency at the design point.

Fig. 4 Comparison of head coefficient and hydraulic efficiency under different time steps

Where R_b denotes the mean bubble radius, P_b represents the saturation vapor pressure, P_l is the liquid density, S is the surface tension coefficient, μ signifies the dynamic viscosity coefficient.

The constant values for the two-phase flow parameters have been defined (Ruggeri & Moore, 1969; Bakir et al., 2004): the Cavitation Vaporization Coefficient was set as 50; the Maximum Density Ratio was set as 1000; the Cavitation Rate and the mean nucleation site diameter was set as 0.25 and 2×10-6m, respectively, which are suitable for most cavitation simulations. Additionally, the standard k-ε model was applied for numerically computing the turbulent flow in cavitating flows involved in this centrifugal fire pump as well.

Concerning about the inlet and outlet boundary conditions, the pressure must be specified at the inlet boundary so as to induce/suppress the development of cavitation in the model centrifugal fire pump. The inlet total pressure and an outlet constant mass flow rate were therefore assumed, respectively. As vapor is generated as cavitation occurs and develops inside the computational domain of the model fire pump, the initial value of the vapor volume fraction has been set as zero at pump inlet. Additionally, the pitch change between the rotor and stator during the steady-state cavitation simulation was modeled using the Frozen Rotor approach.

Numerical calculations of the whole flow inside the centrifugal fire pump running under low, design and high flow conditions were conducted using ANSYS CFX with the temperature of working fluid equal to 25°C. Meanwhile, all steady simulations of cavitation flow have been initialized by using the converged results of the relevant non-cavitation simulation obtained at the same flow rates. The rotating speed of the model fire pump was set at a value of 2960 rpm during all the calculations. Table 3 shows some of the main numerical simulation Settings.

Table 3 Numerical simulation settings

Steps	Numerical Simulation Settings
Cavitation model	Rayleigh-Plesset
Numerical simulation settings	standard k–ε model
Steady state calculation	Frozen Rotor
Data interpolation	General Grid Interface
Inlet boundary condition	Pressure
Outlet boundary condition	Mass flow rate
Steady calculation convergence residuals	10^{-7}
Minimum number of iterations	2
Maximum number of iterations	20

3. EXPERIMENTAL APPARATUS

Based on steady-state numerical results (using the *Frozen Rotor* interface treatment), this study further analyzed the hydraulic performance of the model pump through systematic experiments. Steady-state simulations provided initial flow fields for experimental condition selection and subsequent unsteady calculations. Hydraulic performance tests were conducted at eight flow rates (50%–120% of Q_d=120 m^3/h, i.e., 60–144 m^3/h), covering typical flow regimes such as low-flow backflow, design-

(a) Test section for hydraulic performances of the model fire pump.

(b) the tested centrifugal fire pump

Fig. 5 Test rigs for the measurement of hydraulic performances of the centrifugal fire pumps

point operation, and high-flow shear-layer instability. A range of experiments were conducted in the laboratory of KQ PUMPS, whose testing facilities and measurement technology are sufficient to meet specific requirements (International Organization for Standardization, 1999). The simplified configuration picture for the hydraulic performance test are shown in Fig. 5(a). Moreover, the combined allowable uncertainty of efficiency with respect to the hydraulic performance test rigs in KQ PUMPS is lower than the 0.3% precision class and the random uncertainty is within the 0.1% precision class with respect to the measurement of pressure differences between pump inlet and outlet.

To estimate hydraulic performances of the centrifugal fire pump in this experiment, a couple of intelligent differential pressure sensors (3051CD, 0 ~ 1.6MPa operating range, 0.075% precision class) were used to measure the pressure rise between the pump inlet and pump outlet. Regarding measuring the volumetric flow rate, a discharge electromagnetic flow meter (OPTIFLUX2300W.400, 0~1000*l*/s operating range, 0.15 % precision class) was installed on the discharge line of the water loop to provide measurements of the outlet flow rate. The shaft rotating speed was measured by a smart rotational meter (HBM, K-T40b-002R, 0~2kN m operating range, 0.05% precision class). A series of hydraulic performance tests were conducted in water at room temperature with different flow rates by adjusting the throttle valve in the discharge section.

Pump inlet pressure: The low-pressure measuring point was placed at two impeller inlet diameters upstream in the suction pipeline; Pump pressure rise: The high-pressure measuring point was located at two impeller inlet diameters downstream in the discharge pipeline.

The running parameters of the tested fire pump applied in the experiment are the same as the numerical model with the impeller manufactured using precision casting mold, as shown in Fig. 5(b). The measured hydraulic performances were evaluated by means of the total head coefficient and hydraulic efficiency as a function of the flow rate in fire pump performance tests. The test data of the centrifugal fire pump at various flow rates were illustrated for later comparison with their relevant numerical data.

4. RESULTS AND DISCUSSION

4.1 Investigation of Steady Flow in the Model Fire Pump

Firstly, hydraulic performances of the tested centrifugal fire pump were experimentally investigated to evaluate the overall performance at various flow rates which are 50%, 60%, 70%, 80%, 90%, 100%, 110% and 120% of the design point Q_d, respectively. Furthermore, a series of steady numerical simulations were conducted to predict hydraulic performances of the model fire pump running at the same flow rates.

Particularly, the effect of the selected turbulence models which are standard κ-ε, RNG k-ε and SST k-ω, respectively, on the head coefficient and hydraulic efficiency of the centrifugal fire pump operating at the design point, were analyzed so as to further verify the predicting accuracy in comparison with the experimental results. As illustrated in Table 4, it is apparent that the head coefficient and hydraulic efficiency predicted by using the standard k-ε turbulence model is more consistent with the relevant test data, and the deviation in between is smallest and below 1%. Therefore, the standard k-ε turbulence model was applied later for all numerical calculations in the present study.

Table 4 Influence of turbulence models on the head coefficient and hydraulic efficiency of the centrifugal pump

Turbulence models	Head coefficient	Deviation between CFD and experiment	Hydraulic efficiency (%)	Deviation CFD and experiment
standard *κ-ε*	0.4216	0.36%	79.1	0.75%
RNG *k-ε*	0.4258	0.64%	80.41	2.41%
SST *k-ω*	0.4255	0.57%	80.48	2.51%
Experiment	0.4231	/	78.51	/

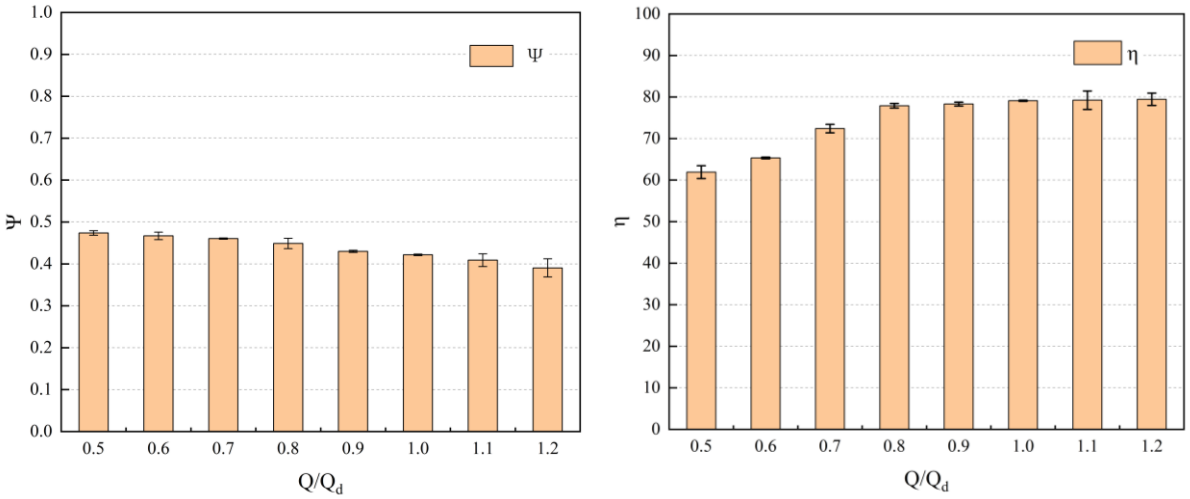

Fig. 6 Comparison of pump performances of the centrifugal fire pump

Accordingly, the relevant experimental data obtained from hydraulic performance test of the model fire pump have been finally analyzed to further confirm the relevant computational results. The predicted hydraulic performance was compared with the corresponding test data of the model fire pump operating at the investigated flow rates as shown Fig. 6. Figure 6 shows the variation trends of the head and hydraulic efficiency of the centrifugal fire pump with flow rate. In addition, the deviations in hydraulic performance between the numerical calculations and experimental data were also examined.

As expected, as the flow rate increases, the pumping characteristic H-Q and hydraulic efficiency characteristic η-Q curves obtained from both numerical simulations and experiment almost show coincidence with each other at lower and design flow rates. Especially, the deviation values of the head coefficient and hydraulic efficiency at the design point are 0.18% and 0.13%, respectively. When the flow rate was higher than 100% of Q_d, there are slight discrepancies occurring at the higher flow rates equal to 120% and 110% of the design value among these curves. In accordance with these two higher flow rates, the corresponding maximum deviations of the head coefficient and hydraulic efficiency are 2.17% and 2.12%, respectively, as can be clearly seen in Fig. 6.

Moreover, the minimum value of the hydraulic efficiency deviation is 0.13% occurring at the design flow point as expected, while at the lower flow rate equal to 50% of Q_d, the hydraulic efficiency deviation value was as large as 1.54%, and it is probably that the intensive unstable flow like prerotation or backflow involved in the pump inlet showed significant hydraulic losses and reduce the hydraulic efficiency at this flow rate during the hydraulic performance test.

Generally, the calculated performance curves of the model fire pump are consistent with the tested ones among most of the investigated flow rates, which indicates that they are in consistence with the experimental data.

4.2 Comparison of Flow Patterns Inside the Model Fire Pump Under Different Flow Conditions

Considering the previously stated details regarding the fire pump's performance, it has been observed that the discrepancies between the predicted and experimental hydraulic performances at the lower and higher flow rates were relatively larger than those at design flow point. Especially, the value of static pressure within the pump under some certain conditions has been always an important factor during the generation of the unstable flow status like cavitation. Since the pressure and velocity gradients are related to the complex inner flow patterns in the impeller, the pressure and velocity distributions in the pump have been therefore analyzed with respect to the investigated flow rates of 60%, 80%, 100% and 120% of Q_d.

In addition, as previously discussed, design point pressure spatial distribution had to be analyzed as well. Figure 7(a), with fewer pressure gradients occurring for the pump in comparison to those operating under lower or high flow conditions. With respect to the relative velocity distribution at the same flow condition as demonstrated in Fig. 7(b), the velocity distribution in the impeller shows more uniform and stable than those at off-design flow conditions. However, the irregular velocity variation toward the blade suction and pressure side was observed at the lower flow rate of 60% of Q_d where some significant low-velocity regions can be found asymmetrically distributed in blade passages. Moreover, in these particular low-velocity regions, unstable flow phenomena can be involved and possibly associated with significant hydraulic losses due to non-uniform flow patterns, and also vary as the flow rate increases or decreases.

The possible reason for the larger deviation of hydraulic performances may have been the large velocity gradients caused by non-uniform flow occurring on both the suction and pressure sides of each blade of the centrifugal fire pump operating at lower or higher flow points.

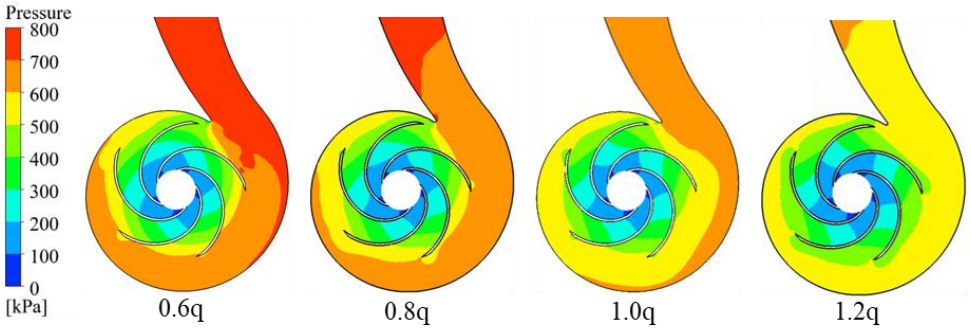

(a) Static pressure distribution in the cross section of the centrifugal fire pump

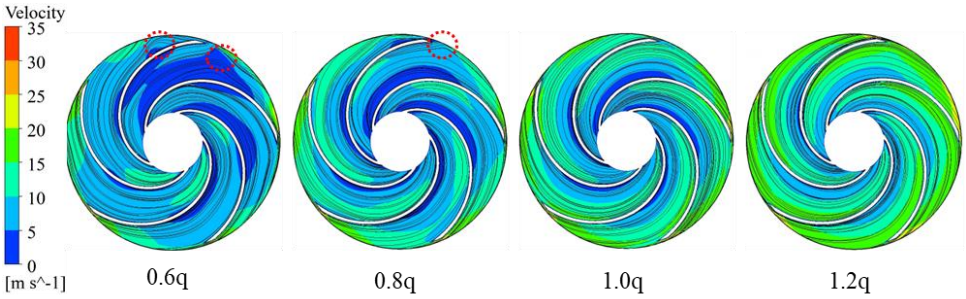

(b) Velocity distribution in the cross section of the centrifugal fire pump

Fig. 7 Comparison of static pressure and relative velocity distribution in the centrifugal pump at different flow rates

4.3 Analysis of Unsteady Flow Analysis in the Centrifugal Fire Pump

To gain further insight on the centrifugal fire pump dynamics, an unsteady flow analysis was conducted on the pump for low, nominal, and high flow rates at 60%, 100%, and 150% of the design flow rate respectively.

4.4 Comparison of Hydraulic Forces Within One Full Rotation of the Impeller

Since the non-uniform flow occurring in the centrifugal fire pump inlet and the rotor-stator interaction can cause periodical variation in the hydraulic forces, which is considered a critical factor for the stable operation of the fire pumps, the hydraulic forces acting on impeller along the radial and axial direction were investigated based upon the unsteady numerical results.

In the current study, the radial hydraulic forces acting on the impeller were considered in the form of the x and y axes. Thus, they were known as Fx and Fy. The axial forces applied to the impellers were acting along the vertical axis as Fz. The coordinate system for illustrating the relevant hydraulic forces acting on the investigated impeller was displayed in Fig. 8(a).

Figure 8(b) displays the hydraulic radial forces acting on the investigated impeller within a full rotation circle at different flow rates. During one full revolution of the impeller, the pattern of all radial forces acting on the impeller is found to have a consistent and symmetric arrangement about the axis in the closed interval distribution of a pentagon for the corresponding flow rates. The magnitude of the radial forces acting on the impeller operating at lower flow rate was larger along the same direction of the axis, indicating that the excited flow forces at lower flow rate are much larger. Moreover, according to the design flow, the radial forces shows smaller indicating that the stability of the rotor system was better and can possibly improve the hydraulic efficiency, which is consistent with the hydraulic efficiency curves and flow patterns at the design flow point as seen in Fig. 7, where the pressure and velocity distribution shows more regular.

Based on the circulation of one rotation cycle, each of the analyzed flow rates has five peaks and five valleys corresponding to the number of blades in the impeller—shown in Fig. 8(c). Moreover, the levels of axial forces acting on the impeller at the lowest flow rate were much more drastic relative to the mean value.

4.5 Pressure Pulsations in the Model Fire Pump Working Under Different Flow Conditions

Based on the analysis of the hydraulic forces in the model fire pump, it was determined that the inner flow within the pump could be unstable especially at lower flow rates. Therefore, the unsteady flow characteristics of the pump were further analyzed by carrying out a range of unsteady numerical simulations. The monitor points of the pressure fluctuation were placed in rotating domain of the impeller outlet and the volute outlet, respectively. What's more, the monitor points located at the five blade passages were numbered gradually along the impeller rotation direction as displayed in Fig. 9.

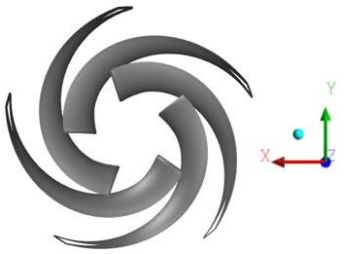

(a) The coordinate system of impellers for the hydraulic force analysis

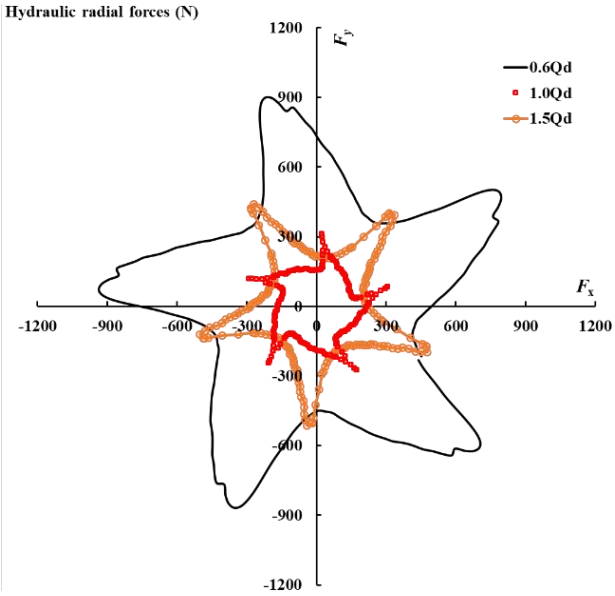

(b) Comparison of hydraulic radial forces at different flow rates

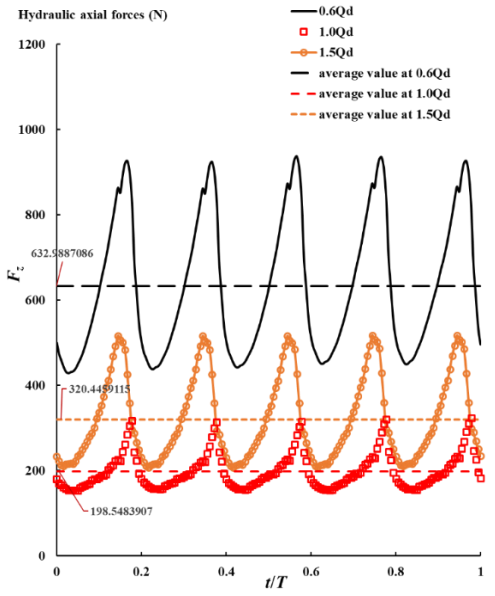

(c) Comparison of hydraulic axial forces at different flow rates

Fig. 8 Hydraulic l forces acting on the impeller of the centrifugal fire pump at different flow rates

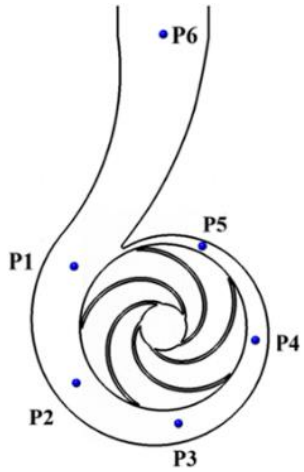

Fig. 9 Location of monitor points at impeller outlet

In addition, a dimensionless pressure coefficient C_p has been employed in pressure pulsation analysis with its expression shown as follows,

$$C_p = \frac{p - \overline{p}}{0.5\rho u_2^2} \tag{8}$$

Where p represents the transient value of the static pressure of the monitor point, Pa; $\overline{p}$ denotes the average static pressure at the monitoring point within one full rotating circle of the impeller, Pa.

The fast fourier transformation of the unsteady pressure signals collected from the impeller outlet at the investigated flow rates which correspond to 60%, 100% and 150% of Q_d, was obtained for comparison as well. The time domain analysis of pressure fluctuations in impeller outlet and volute outlet at lower, design and higher flow rates have been demonstrated in Figes 10 and 11.

As expected, yielding to the rotor-stator interaction between the impeller and the volute, the pressure variation for each monitor point had a periodic characteristic and similar to a regular sinusoidal curve where there were five peaks and five valleys within one rotating circle of the impeller, which is consistent with the blade number of the fire pump. Clearly, it can be observed that the more the location of the monitor points (such as monitor points of P1 and P5) is close to the flow area near the volute tongue, the more intense pressure pulsations are, and the more significant this feature is as observed at off-design flow rates, which is consistent with the amplitude distribution of dominant frequencies of pressure pulsations obtained at different positions in the impeller out, as seen in Fig. 14.

Moreover, at the design flow point, the magnitude of the pressure variation in both the impeller and volute outlet was in more harmony than those at lower and higher

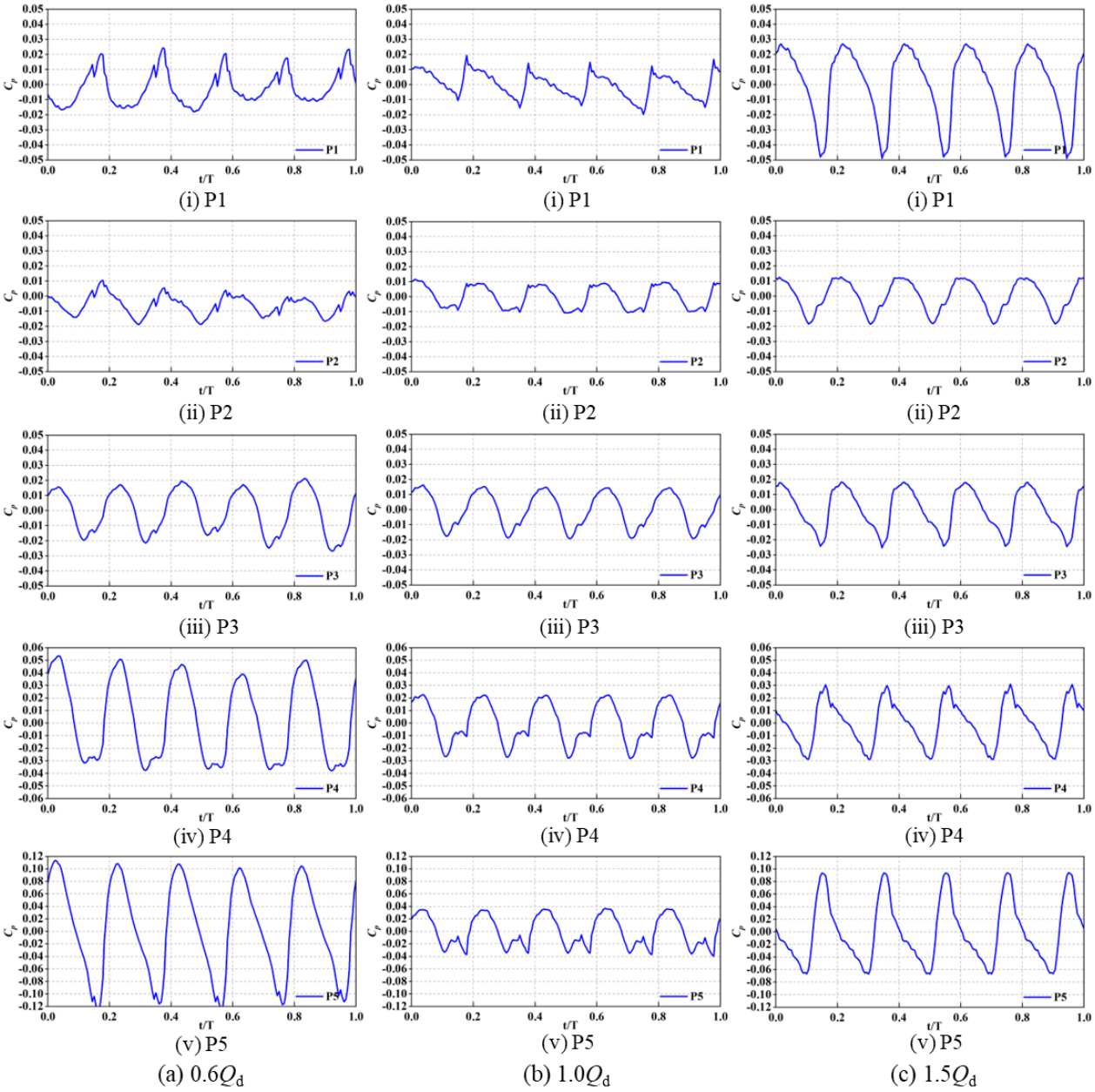

Fig. 10 Time domain analysis of pressure pulsations at impeller outlet

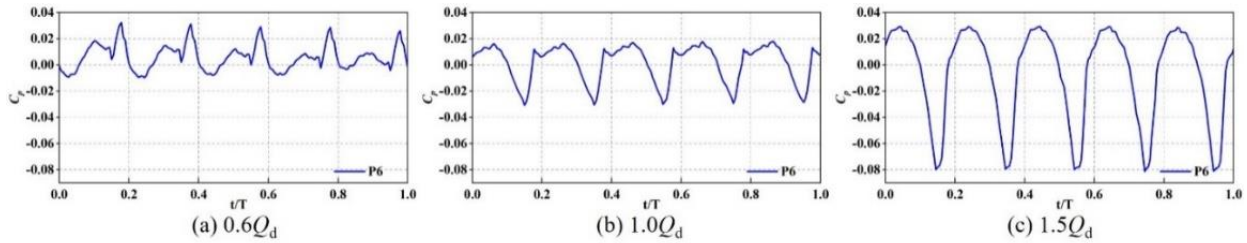

Fig. 11 Time domain analysis of pressure pulsations at volute outlet

flow rates, indicating that the internal flow in the model fire pump turned out to be more uniform than those at the other two flow rates, which is also in accordance with the previous conclusion of the hydraulic force analysis for the same flow rate.

In regard to studying the pressure oscillation spectra in the impeller outlet and volute outlet at the monitored flow rates, the studied frequencies in the x-axis up to 3000 Hz were analyzed as seen in Fig. 12 and Fig. 13. It was noticed that at the flow rates of 60%, 100% and 150% of designed flow point, there were some overriding prominent peaks marked in between the oscillation band of pressure signal in the impeller outlet and volute outlet. These centers corresponded to the fundamental and first overtone.

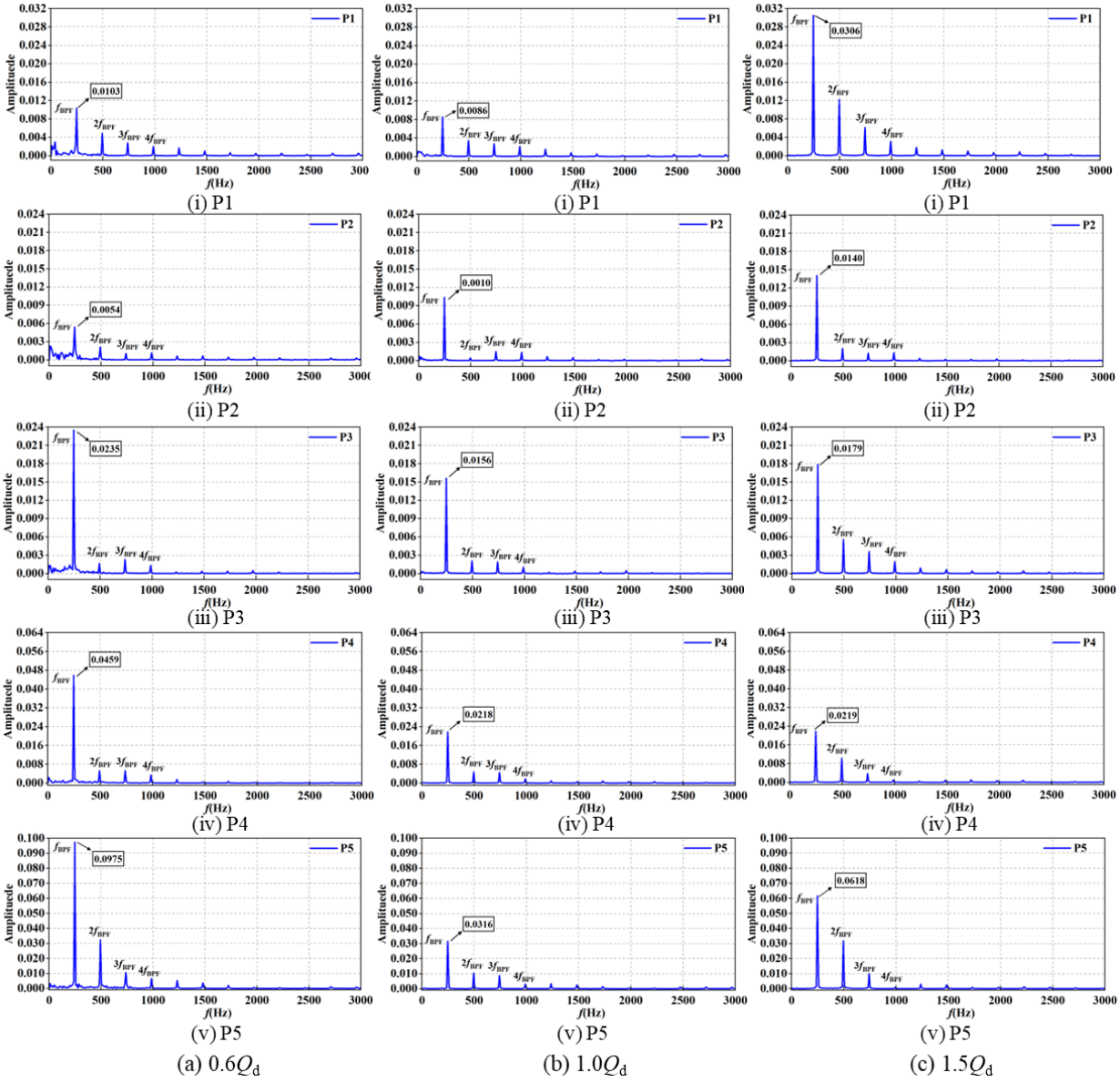

Fig. 12 Frequency domain analysis of pressure pulsations at impeller outlet

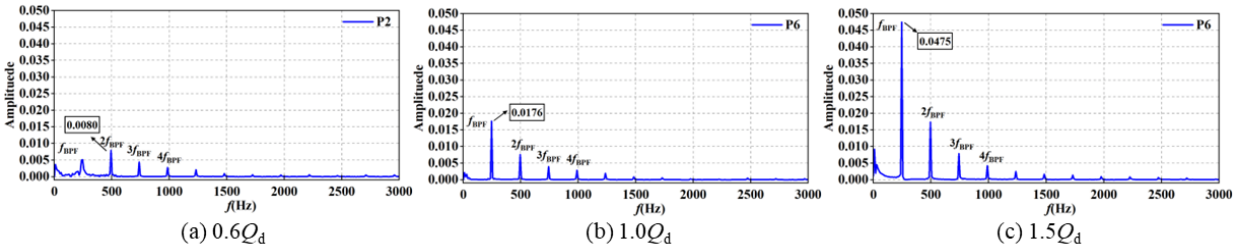

Fig. 13 Frequency domain analysis of pressure pulsations at volute outlet

Specifically, with respect to pressure pulsations at impeller outlet, the same main frequency of 247.3 Hz is observed for all the monitor points at the investigated low, design and high flow rate, and is equal to the blade passing frequency (247Hz). The secondary main frequencies observed for all the monitor points in the impeller outlet are 494.5Hz which is almost 2 times of the blade passing frequency at the flow rates equal to 60% and 150% of the design flow point. However, at the design point, the second main frequency of pressure pulsations at the position of monitor point P2 is 741.75 Hz, which is different from the value of 494.5Hz obtained for other monitor points located in the impeller outlet.

Particularly, at the lower flow rate of 60% of Q_d, the third main frequencies of pressure pulsations observed at monitor points of P1, P2 and P6 located at the impeller

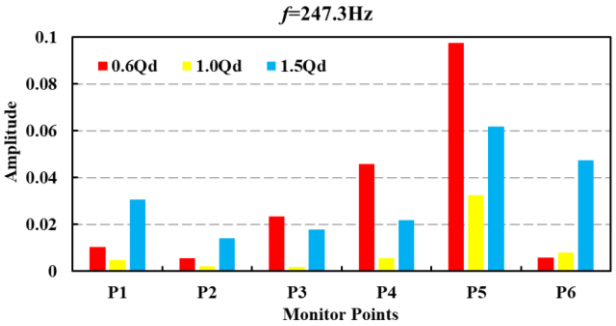

(a) Comparison of amplitudes of the frequency equal to 247.3Hz

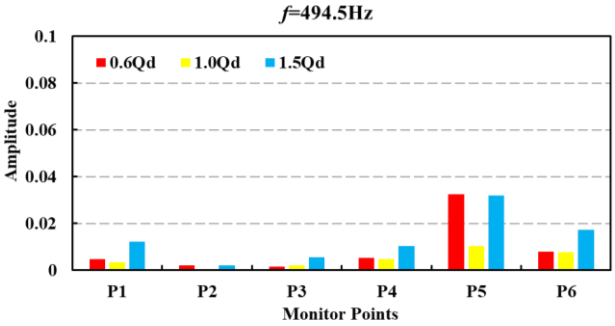

(b) Comparison of amplitudes of the frequency equal to 494.5Hz

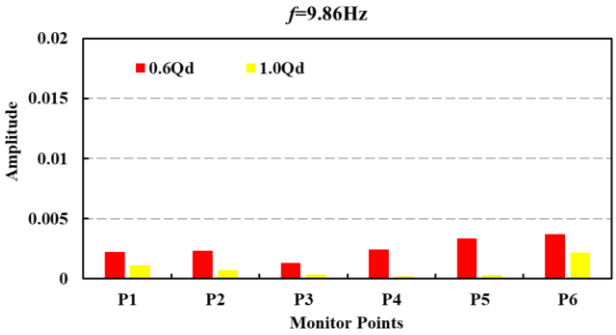

(c) Comparison of amplitudes of the frequency equal to 9.86Hz at design and high flow rates

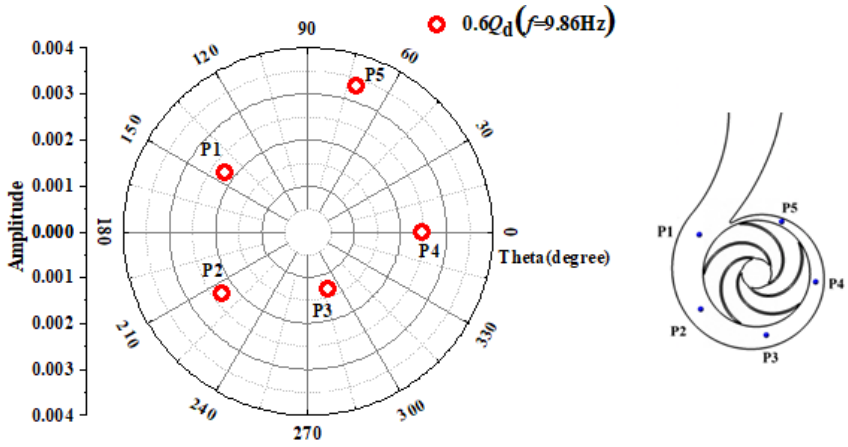

(d) Comparison of amplitudes of the frequency equal to 9.86Hz at the lower flow rate

Fig. 14 Comparison of amplitudes of dominant frequencies of pressure pulsations in the model fire pump

outlet are 9.86Hz, 39.4Hz and 9.86Hz, respectively. These frequencies are obviously lower than the impeller rotational frequency which is equal to 49.3 Hz, and aren't dominant in the pressure fluctuations of other monitor points especially at design and high flow rates.

Additionally, comparison of amplitudes of the dominant frequencies equal to 247.Hz and 494.5Hz obtained among the investigated monitor points at both impeller out and volute outlet was carried out among different flow rates, as shown in Fig. 14(a) and 14(b). Clearly, at the design flow rate, the amplitudes of these two dominant frequencies corresponding to the pressure pulsations of all the monitor points are smaller than those at low and high flow rates. Meanwhile, the variation of these amplitudes is quite flat with smaller differences observed among different monitor points, indicating that the inner flow inside the centrifugal fire pump is more stable and uniform under the design flow condition.

However, with respect to these two investigated dominant frequencies obtained at the position of monitor point P5 in the impeller outlet, their corresponding amplitudes are much larger than those obtained at other monitor points among all the flow rates, indicating that there are strongest pressure pulsations occurring at this area near the volute tongue as shown in Fig. 14(a) and 14(b). Especially, these amplitudes reach their maximum values at the lower flow rate of 60% of Q_d, and it could be the possible unstable flow phenomena with most intensive pressure pulsations occurring in the model fire pump running under this lower flow condition.

As discussed above, the third main frequencies equal to 9.86Hz were only observed occurring in the frequency domain of pressure fluctuations obtained at monitor points of P1 and P6 under the lower flow rate equal to 60% of the design point. Therefore, the amplitudes of this particular low frequency of f=9.86 Hz were further analyzed and compared among different monitor points located both in the impeller outlet and volute outlet under the investigated lower and design flow conditions, as illustrated in Fig. 14(c) and Fig. 14(d). Obviously, the corresponding amplitudes of this low frequency according to all the monitor points are larger than those obtained at design flow rate as shown in Fig. 14(c). The characteristic of low-frequency and intensive energy observed in the pressure pulsations isn't typical obtained even from the same monitor points at design or higher flow rates.

Moreover, the amplitude of this particular frequency equal to 9.86 Hz obtained at monitor point P6 which is located in the volute is larger than those obtained at monitor points located in the impeller, indicating that the flow phenomena associated with this low frequency has a significant influence on the flow inside the volute. At the same time, as observed in Fig. 14(d), the amplitude of this frequency obtained at the position of monitor point P1 is smaller than that obtained at the position of monitor point P5 where strong rotor-stator interaction occurs, and this is consistent with the observation in time domain analysis in Fig. 10.

4.6 Analysis of Cavitating Flow in the Centrifugal Fire Pump

The investigations on the fire pump cavitation showed that for the selected flow rates of 60%, 100%, and 150% of Qd, the cavitation performance characteristics curves were determined. The estimates of cavitation performance characteristics were obtained by determining the head coefficient as a function of the cavitation number at constant flow rates. The cavitation number (σ) was calculated using the following equation:

$$\sigma = \frac{p_{in} - p_v}{0.5\rho u_1^2} \tag{9}$$

Where p_{in} is the pump inlet static pressure, Pa; p_v is the saturated vapor pressure of water at 25°C, a p_v=3574Pa; u_1 is the mean velocity at the impeller inlet. The comparison of the head-drop curves among different flow conditions can be therefore conducted, as indicated in Fig. 15.

4.7 Comparison of Cavitation Performance Curves of the Model Fire Pump

Generally, with respect to all three investigated flow rates, with the initial cavitation number σ starting to decrease, the head coefficient value Ψ gradually decreases, as observed in Fig. 15. However, for the higher flow condition of 150% of the design point, the cavitation effect on the head coefficient becomes more significant, since the value of cavitation number σ at which the initial head coefficient begins to decrease gradually increases in comparison with those at lower and design flow rates, and the head-drop rate is relatively slower. For example, at the lower flow rate of 60% of Qd, the head

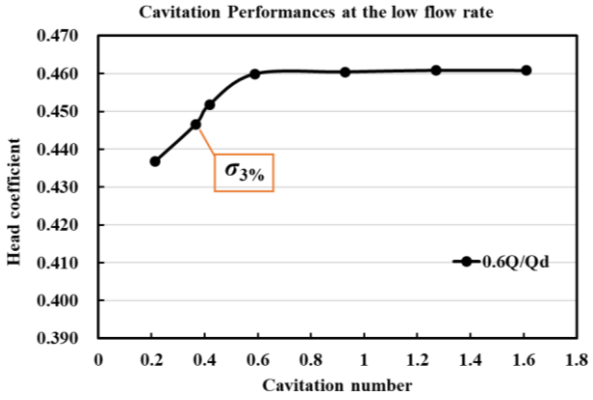

(a) 60 of Q_d

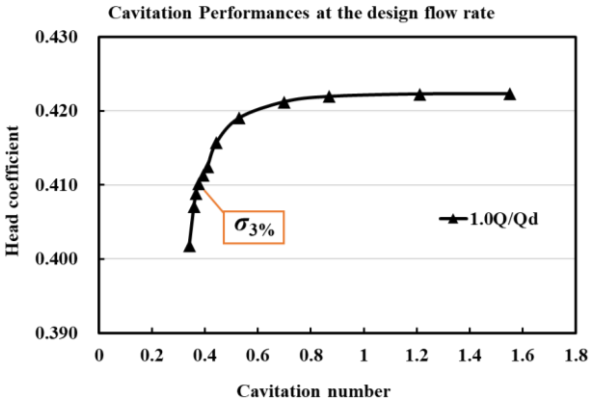

(b) 100 of Q_d

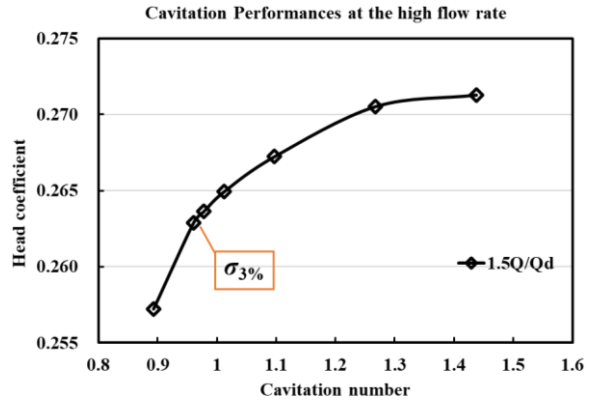

(c) 150 of Q_d

Fig. 15 Cavitation performances of the centrifugal fire pump at different flow rates

coefficient decreases when σ = 0.586. For the design and high flow cases, the corresponding values of σ are 0.87 and 1.26, respectively. Particularly, a significant observation has been identified on the cavitation performance curve of the centrifugal fire pump: with respect to the pump head-drop amount equal to 3%, as the flow rate increases, the values of the corresponding cavitation number $\sigma_{3\%}$ increase, and they are 0.366, 0.376 and 0.961 for the investigated low, design and high flow conditions, respectively.

5. CONCLUSIONS

This study presents comprehensive findings on hydraulic performances, cavitation behavior, and pressure

pulsations inside the centrifugal fire pump across various flow rates, derived from numerical simulations combined with experimental investigations. Additionally, a series of detailed time and frequency domain analysis of the unsteady flow within the fire pump revealed differences in dynamic characteristics of the inner flow in the model fire pump running at lower flow conditions compared to the design flow condition, particularly in terms of the onset of low-frequency pressure pulsations. From these analyses, the conclusions can be drawn as follows:

In light of the interrogation of the influence of the standard turbulence models $\varkappa-\varepsilon$, RNG k−ε, and SST k−ω on the numerical results, it can be deduced that the standard $\varkappa-\varepsilon$ turbulence model is the best option for predicting the efficiency of the fire centrifugal pump since it showed the least divergency from the measurement results.

The performance curves of the centrifugal fire pump calculated alongside the experiments retain reasonable alignment across a broad span of flow rates Notably, at and below the design point, the deviations within hydraulic performances between the predicted and tested data were below 1.6%. In contrast, at higher flow rates, the corresponding deviations were around 2%. At a lower flow rate of 50% of Q_d, the hydraulic efficiency exhibited a deviation of 1.54%. This discrepancy can be attributed to the presence of intense unstable flow conditions, such as prerotation or backflow, at the pump inlet during testing. These unstable flow phenomena contributed to increased hydraulic losses and consequently reduced hydraulic efficiency at this particular flow rate.

Within a period of one rotating circle of the impeller, the distribution of the hydraulic radial forces acting on the impeller shows a regular and symmetric shape for the investigated low, design and high flow rates. Larger magnitude of the radial forces was further observed at lower flow rate indicated that there are larger excited flow forces acting on the impeller which probably induce an unstable rotor system and reduce the hydraulic efficiency at the same time. This significant observation is also consistent with the irregular distribution of static pressure and velocity in the impeller as analyzed.

Regarding the hydraulic axial forces acting on the impeller over one rotating cycle, it was observed that for all investigated flow rates, there were five peaks and five valleys, in alignment with the blade number. Particularly, at lower flow rates, the magnitude of the axial forces exhibited a greater variation around the average value, coinciding with the observation of pressure pulsations in the impeller outlet at these lower flow rates.

Concerning the analysis of pressure fluctuations within the impeller outlet and volute outlet in both the time and frequency domains, it was found that the static pressure exhibited a periodic variation over time. The primary frequencies were different in the frequency domain for both the impeller outlet and the volute outlet. Specifically, under the investigated low, design, and high flow conditions, the main frequency in the impeller outlet was the blade passing frequency (fb = 247.3 Hz), whereas in the volute outlet, the main frequencies were approximately twice that of fb. Notably, at a low flow rate of 60% of Q_d, the third main frequency of pressure pulsations in both the impeller outlet and volute outlet was 9.86 Hz, which is lower than the impeller rotational frequency but possesses significant energy. This suggests that the occurrence of possible backflow at lower flow rates has a more pronounced impact on pressure pulsations.

In regard to the performance of centrifugal fire pump regarding cavitation ,thire is a distinict phenomenon evident on the cavitation curve: when the pump head-drop amount equals 3%, an increase in flow rate results in corresponding increases in the cavitation number σ3%. Specifically, for the investigated low, design, and high flow rates, the values of σ3% are 0.366, 0.376, and 0.961, respectively.

To improve the efficiency and operational reliability of centrifugal fire pumps, centrifugal pump fire simulations offer several suggestions based on their numerical simulations. It is advised to maintain the flow rate close to the design flow rate during operation to ensure optimal hydraulic efficiency and minimize pressure pulsations. The risk of cavitation can be mitigated by increasing the pump inlet pressure or refining the impeller geometry to enhance the cavitation number. To address the significant pressure pulsations at low flow rates, design modifications such as optimizing the impeller stagger angle or the volute tongue geometry, along with the use of diffusers or anti-surge mechanisms, are recommended to stabilize the flow. Additionally, the implementation of balanced impeller designs or the addition of appropriate bearings can help counteract hydraulic forces and improve rotor system stability. These conclusions provide a theoretical basis for optimizing the design and operation of centrifugal fire pumps, thereby enhancing the reliability and efficiency of fire protection systems.

In summary, the anticipated hydraulic performances of the model fire pump are consistent with the corresponding test data across a broad spectrum of flow rates. This alignment underscores the capability of the current numerical methods in the present work to accurately capture the inner flow within centrifugal fire pumps. Consequently, the numerical method employed in this study serves as an effective tool for comprehending, analyzing, predicting, and managing the intricate mechanisms associated with centrifugal fire pump operation under a wide array of design and off-design conditions.

ACKNOWLEDGEMENTS

Jiangsu University Senior Personnel Scientific Research Foundation (No.15JDG073) awarded the study's funding together with The Open Research Subject of Key Laboratory (Research Base) of Key Laboratory of Fluid and Power Machinery, Ministry of Education (No.szjj2016-065) and The Priority Academic Program Development of Jiangsu Higher Education Institutions.

CONFLICT OF INTEREST

The authors have no competing interests or conflicts to disclose.

AUTHORS CONTRIBUTION

Jialin Hao and **Yanxia Fu:** Conceptualization; methodology; formal analysis; writing original draft. **Chenxin Yu**, **Peiyi Zhang**, **Duohua Hou**, **Yang Shen**, and **Jianpin Yuan**: writing review and editing. All authors have read and agreed to the published version of the manuscript.

REFERENCES

Elyamin, G. R. A., Bassily, M. A., Khalil, K. Y., & Gomaa, M. S. (2019). Effect of impeller blades number on the performance of a centrifugal pump. *Alexandria Engineering Journal, 58*(1), 39-48. https://doi.org/10.1016/j.aej.2019.02.004

ANSYS Inc. (2012). *Theory Reference*. ANSYS Inc.

Bakir, F., Rey, R., Gerber, A. G., Belamri, T., & Hutchinson, B. (2004). Numerical and experimental investigations of the cavitating behavior of an inducer. *International Journal of Rotating Machinery*, *10*(1), 15-25. https://doi.org/10.1155/s1023621x04000028

Bozorgasareh, H., Khalesi, J., Jafari, M., & Gazori, H. O. (2021). Performance improvement of mixed-flow centrifugal pumps with new impeller shrouds: numerical and experimental investigations. *Renewable Energy*, *163*(Pta1), 635-648. https://doi.org/10.1016/j.renene.2020.08.104

Brennen, C. E. (2012). *A review of the dynamics of cavitating pumps.* IOP Conference Series Earth and Environmental Science, 15(1), 2001. https://doi.org/10.1088/1755-1315/15/1/012001

Dai, C., Ge, Z., Dong, L., & Zhu, J. (2022). Study on noise characteristics of marine centrifugal pump under different cavitation stages. *Iranian Journal of Science and Technology, Transactions of Mechanical Engineering*, 1-15. https://doi.org/10.1007/s40997-020-00390-5

Fu, Y., Fang, Y., Yuan, J., Yuan, S., Pace, G., & Dagostino, L. (2016). Study on Hydraulic Performances of a 3 - Bladed Inducer Based on Different Numerical and Experimental Methods. *International Journal of Rotating Machinery, 2016*(1), 4267429. https://doi.org/10.1155/2016/4267429

Fu, Y., Fan, M., Pace, G., Valentini, D., Pasini, A., & d'Agostino, L. (2018, July). *Experimental and numerical study on hydraulic performances of a turbopump with and without an inducer*. Fluids Engineering Division Summer Meeting (Vol. 51579, p. V003T12A032). American Society of Mechanical Engineers. https://doi.org/10.1115/FEDSM2018-83506

Huan, Y. Y., Liu, Y. Y., Li, X. J., Zhu, Z. C., Qu, J. T., Zhe, L., & Han, A. D. (2021). Experimental and numerical investigations of cavitation evolution in a high-speed centrifugal pump with inducer. *Journal of Hydrodynamics, 33*(1), 140-149. https://doi.org/10.1007/s42241-021-0006-z

International Organization for Standardization (1999). *ISO 9906:1999 - Rotodynamic pumps — Hydraulic performance acceptance tests — Grades 1 and 2*. https://doi.org/10.3403/30202352

Jia, X., Yang, X., & Zhu, Z. (2024). Study on pressure pulsations and transient fluid forces in centrifugal pump under different degrees of cavitation. *Proceedings of the Institution of Mechanical Engineers, Part E: Journal of Process Mechanical Engineering, 238*(6), 2834-2844. https://doi.org/=10.1177/09544089231164832

Long, Y., An, C., Zhu, R., & Chen, J. (2021). Research on hydrodynamics of high velocity regions in a water-jet pump based on experimental and numerical calculations at different cavitation conditions. *Physics of Fluids, 33*(4). https://doi.org/10.1063/5.0040618

Lu, J., Chen, Q., Liu, X., Zhu, B., & Yuan, S. (2022). Investigation on pressure fluctuations induced by flow instabilities in a centrifugal pump. *Ocean Engineering, 258*, 111805. https://doi.org/10.1016/j.oceaneng.2022.111805

Lu, J., Liu, J., Qian, L., Liu, X., Yuan, S., Zhu, B., & Dai, Y. (2023). Investigation of pressure pulsation induced by quasi-steady cavitation in a centrifugal pump. *Physics of Fluids, 35* (2), 025119.https://doi.org/10.1063/5.0135095

Nolan, D. P. (2011). Fire fighting pumping systems at industrial facilities. *Fire Fighting Pumping Systems at Industrial Facilities*, 215–220. https://doi.org/10.1016/B978-081551428-2.50025-X

Oro, J. M. F., Perotti, R. B., Vega, M. G., & Gonzalez, J. (2023). Effect of the radial gap size on the deterministic flow in a centrifugal pump due to impeller-tongue interactions. *Energy, 278*, 127820. https://doi.org/10.47176/jafm.15.06.1303

Osman, F. K., Zhang, J., Lai, L., & Kwarteng, A. A. (2022). Effects of turbulence models on flow characteristics of a vertical fire pump. *Journal of Applied Fluid Mechanics, 15*(6), 1661-1674. https://doi.org/10.47176/jafm.15.06.1303

Palgrave, R. (2003). *Troubleshooting Centrifugal Pumps And Their Systems.* 1-I. https://doi.org/10.1016/B978-185617391-9/50018-6

Ramirez, R., Avila, E., Lopez, L., Bula, A., & Forero, J. D. (2020). CFD characterization and optimization of the cavitation phenomenon in dredging centrifugal pumps. *Alexandria Engineering Journal*, *59*(1), 291-309. https://doi.org/10.1016/j.aej.2019.12.041

Ruggeri, R. S., & Moore, R. D. (1969). Method for prediction of pump cavitation performance for

various liquids, liquid temperatures, and rotative speeds. *National Aeronautics and Space Administration.*

Skrzypacz, J., J., & Bieganowski, M. (2018). The influence of micro grooves on the parameters of the centrifugal pump impeller. *International Journal of Mechanical Sciences, 144*, 827-835. https://doi.org/10.1016/j.ijmecsci.2017.01.039

Sonawat, A., Kim, S., Ma, S. B., Kim, S. J., Lee, J. B., Yu, M. S., & Kim, J. H. (2022). Investigation of unsteady pressure fluctuations and methods for its suppression for a double suction centrifugal pump. *Energy, 252*, 124020. https://doi.org/10.1016/j.energy.2022.124020

Song, Y., Zhang, T., Liu, Q., Ge, B., Liu, J., & Zhang, L. (2024). Cavitation identification method of centrifugal pumps based on signal demodulation and EfficientNet. *Arabian Journal for Science and Engineering,* 1-15. https://doi.org/10.1007/s13369-024-09193-1

International Association of Fire and Rescue Services (CTIF). (2014). World fire statistics: Information bulletin of the World (Report No. 19). https://mail.ctif.org/sites/default/files/ctif_report19_world_fire_statistics_2014.pdf

Xianwei, L. I. U., Jiangfeng, F. U., Junjie, Y. A. N. G., Dewen, Y. I. N., Zhenhua, Z. H. O. U., & Huacong, L. I. (2024). Numerical simulation research on multiphase flow of aviation centrifugal pump based on OpenFOAM. *Chinese Journal of Aeronautics, 37*(4), 256-275. https://doi.org/10.1016/j.cja.2023.11.016

Yousefi, H., Noorollahi, Y., Tahani, M., Fahimi, R., & Saremian, S. (2019). Numerical simulation for obtaining optimal impeller's blade parameters of a centrifugal pump for high-viscosity fluid pumping. *Sustainable Energy Technologies and Assessments*, *34*(AUG.), 16-26. https://doi.org/10.1016/j.seta.2019.04.011

Zhu, Y., Zhou, L., Lv, S., Shi, W., Ni, H., Li, X., ... & Hou, Z. (2023). Research progress on identification and suppression methods for monitoring the cavitation state of centrifugal pumps. *Water*, *16*(1), 52. https://doi.org/10.3390/w16010052.